Article

Effects of rubidium fluoride and potassium fluoride post deposition treatments on Cu(In,Ga)Se2 thin films and solar cell performance

Enrico Avancini, Romain Carron, Thomas P. Weiss, Christian Andres, Melanie Bürki, Claudia Schreiner, Renato Figi, Yaroslav E. Romanyuk, Stephan Buecheler, and Ayodhya N. Tiwari

Chem. Mater., **Just Accepted Manuscript** • DOI: 10.1021/acs.chemmater.7b03412 • Publication Date (Web): 22 Oct 2017

Effects of rubidium fluoride and potassium fluoride post deposition treatments on $Cu(In,Ga)Se_2$ thin films and solar cell performance

Enrico Avancini[1], Romain Carron[1], Thomas P. Weiss[1], Christian Andres[1], Melanie Bürki[2], Claudia Schreiner[2], Renato Figi[2], Yaroslav E. Romanyuk[1], Stephan Buecheler[1] and Ayodhya N. Tiwari[1].

[1]Laboratory for Thin Films and Photovoltaics, Empa - Swiss Federal Laboratories for Materials Science and Technology, Ueberlandstrasse 129, CH-8600 Duebendorf, Switzerland

[2]Laboratory for Advanced Analytical Technology, Empa - Swiss Federal Laboratories for Materials Science and Technology, Ueberlandstrasse 129, CH-8600 Duebendorf, Switzerland

Abstract

Post-deposition treatments (PDTs) with sodium fluoride (NaF) and potassium fluoride (KF) were introduced as a way to improve the efficiency of $Cu(In,Ga)Se_2$ (CIGS) based solar cells. Here, we apply post-deposition treatments with rubidium fluoride (RbF) to low-temperature co-evaporated CIGS absorbers after a first PDT with sodium fluoride (NaF), and compare the effects of the addition of Rb and K on the solar cell performance and material properties of the CIGS films. KF and RbF PDTs lead to similar improvements in the open circuit voltage (V_{oc}) and fill factor (FF), while allowing a reduction of the thickness of the cadmium sulfide (CdS) buffer layer without loss in electronic performance. KF and RbF lead to comparable modifications of the morphology and composition of the CIGS films. After the PDT, K and Rb accumulate in a nanopatterned copper-poor secondary phase at the CIGS surface, while also diffusing within the CIGS layer and strongly reducing the concentration of lighter alkali element sodium. These findings corroborate theoretical calculations published by another group, which predicted the segregation of potassium indium selenide ($KInSe_2$) and rubidium indium selenide ($RbInSe_2$) at CIGS surfaces under the used PDT conditions.

Introduction

Alkali-fluoride (AlkF) post-deposition treatments (PDTs) with heavy alkali elements led to a surge in efficiency improvements of $Cu(In,Ga)Se_2$ (CIGS) solar cells in recent years. PDTs with potassium fluoride (KF) were introduced in 2013[1] on low-temperature co-evaporated CIGS absorbers grown on flexible substrates. Later, an outstanding record efficiency of 22.6% was obtained with rubidium fluoride (RbF) PDT on high-temperature CIGS[2]. PDT was initially introduced as a mean to incorporate sodium in CIGS films grown on flexible polyimide (PI) substrates[3], and consist in the co-evaporation of selenium and sodium fluoride (NaF) after the deposition of CIGS. This was necessary due to the absence of Na diffusing from the alkali-free substrate and for controlled Na incorporation in the CIGS.

Small amounts of Na, typically in the order of 0.1 at%, are known to increase the net hole concentration in CIGS absorbers, as determined by capacitance-voltage measurements, with a major benefit on the open-circuit voltage (V_{oc}). Benefits of PDTs based on KF include further gains in the V_{oc}[1,4]. In addition, the KF-PDT opened the possibility to reduce the thickness of the CdS buffer layer without degradation of the electronic performance, thereby reducing parasitic absorption by the buffer layer at long wavelengths and thus leading to larger short-circuit currents (J_{sc}). Larger open

circuit voltages were also observed after KF PDTs on cells with alternative Zn(O,S) buffer layers[5] and for CIGS absorbers grown by sequential sputtering and selenization[6].

The incorporation of Na mainly affects the electronic properties of the CIGS bulk, whereas the benefits of KF PDT have also been associated with beneficial modifications of the surface[7]. So far there is no consensus on the mechanism behind the beneficial effect of "heavier" alkaline elements in CIGS solar cells. In an early stage it was proposed that KF PDT enhances Cu depletion of the CIGS surface, promoting Cd incorporation during the deposition of the CdS buffer layer by chemical bath deposition (CBD), which could result in a type inversed CIGS layer beneath the absorber/buffer interface[1,7]. Such compositional modifications were reported also by other groups[8,9]. Investigations of the surface composition and morphology revealed the formation of a Cu-poor, In-, Se- and K- rich "KIS" layer with a thickness of a few nanometers[10]. In combination with a NaF PDT, this can result in a nanopatterned morphology. This concept could be used as a basis for the development of passivated junction with point contacts[11,12]. CIGS layers with the K-In-Se phase on the surface show a significant lowering of the valence band maximum on the surface resulting in increased surface band gap of up to 2.5 eV[13]. This surface layer possibly acts as a hole-blocking layer passivating the CIGS/buffer layer interface. A model proposed by Lepetit[9] suggested that the enhanced Cd incorporation at KF-treated CIGS surfaces could be explained by the transformation of the KIS layer into a $CdIn_2S_4$ phase during CdS-CBD, with the substitution of K and Se by Cd and S, respectively. The electronic and material properties of such post-CBD layer are still unknown and a direct proof missing. Lepetit *et al.* showed that a K-In-Se phase can be intentionally co-evaporated on the CIGS surface, resulting in similar effects as those of KF PDT[14].

Although the effects of potassium incorporation into the CIGS layers are being investigated, several groups have shown that lighter alkali elements are replaced by heavier ones during the PDTs. This was initially observed with the substitution of Na with K[1,10], and was recently also shown by Jackson *et al.* for Rb and Cs replacing K and Na[2]. Subsequent to the KF PDT work[1,15], the use of RbF PDTs was reported by Jackson *et al.*[2] for solar cells grown on glass substrates which provide both K and Na in CIGS during growth at high temperature (approx. 550°C).

As both KF and RbF PDTs have shown solar cell efficiency improvements we further investigated how much different are the influences of the RbF and KF PDTs. Here, we present a comparative study of the CIGS layers to answer the question if by substituting KF PDT with RbF PDT higher efficiencies could be achieved and why.

We first discuss the photovoltaic properties of solar cells based on CIGS absorbers treated by different PDTs with NaF, NaF followed by KF (NaF+KF), and NaF followed by RbF (NaF+RbF). Especially, we focus on the comparison between KF PDT and RbF PDT. The beneficial effects of KF PDTs on the photovoltaic properties of CIGS solar cells could be reproduced with RbF PDT while CIGS absorbers treated only with NaF PDTs yield lower solar cell efficiencies. NaF PDT was used in all absorbers prior to KF or RbF treatment in order to provide the sufficient amount of Na doping, and to make our results more comparable to the cases where Na diffuses in the CIGS layers from soda-lime glass substrates or from a precursor layer prior to the CIGS deposition.

We then carefully measured and analyzed the chemical composition of the surfaces and layers of CIGS treated with different PDTs. Investigations were also performed to test and validate the theoretical predictions based on density functional theory (DFT) calculations about the effects of alkali in CIGS[16].

Experimental

CIGS thin films were deposited on molybdenum-coated soda-lime glass (SLG) substrates by multi-stage co-evaporation of Cu, In and Ga as described in an earlier publication[17]. To prevent uncontrolled diffusion of alkali elements from the substrate, a silicon oxide barrier layer was deposited by pulsed DC magnetron sputtering between the SLG and the molybdenum back contact. In the case of ICP-MS and XPS experiments, the glass substrate was replaced with molybdenum-coated flexible polyimide. The deposition parameters were adjusted so that the quality and composition of the CIGS film is independent on the choice of substrate. An approximately 30 nm thick buffer layer of cadmium sulfide (CdS) was deposited by CBD in a basic environment (2 M [NH_3] in water) at 70°C. Before the CBD bath, the CIGS thin films were rinsed in a similarly concentrated bath of diluted ammonia. Window layers of unintentionally doped zinc oxide (ZnO) and Al-doped (Al_2O_3 2 wt.%) ZnO were deposited by RF magnetron sputtering. Ni/Al grids and MgF_2 anti-reflective coatings were deposited by e-beam evaporation.

Integral [Cu]/([Ga]+[In]) (CGI) and [Ga]/([Ga]+[In]) (GGI) ratios were calculated from the intensity of K alpha lines of Cu, In and Ga in X-ray Fluorescence (XRF) measurements, earlier calibrated using CIGS layers with known CGIs and GGIs.

The current-voltage (J-V) characteristics of completed solar cells were analyzed under an AM 1.5G solar simulator equipped with a Xe lamp. The power density was calibrated to 1000 W/m^2 by measuring the current output of a Si cell with a certified response. The temperature of the solar cell was kept at a constant value of 25°C using PID-controlled Peltier heat pumps. A Keithley 2400 four-probe source meter was used for the measurements. The reported uncertainty on the short-circuit current (J_{sc}) is calculated assuming a maximal error of 2% on the calibration of the power of the solar simulator lamp. The reported uncertainty on the open-circuit voltage is calculated assuming an uncertainty of 1°C on the measurement temperature, propagated on the V_{oc} utilizing the open-circuit diode equation ($V_{oc}=A*kT*\ln(J_{sc}/J_0)$, where kT is the thermal energy, A is the diode quality factor and J_0 is the diode saturation current density). The reported uncertainties on the Fill Factor (FF) and efficiency are calculated by propagating the error on the J_{sc} and V_{oc} utilizing the open-circuit diode equation and the mathematical expressions for the FF and the efficiency. Equal uncertainties are assumed for the J_{sc} and the current density at the maximum power point (J_{mpp}), as well as for the V_{oc} and the voltage at the maximum power point (V_{mpp}). Averages are calculated for the four cells with the highest efficiency in each six-cell sample. The reported error represents the standard deviation, if above the estimated measurement uncertainty on a single-cell measurement. Typical cell area is approximately 0.5 cm^2. The reported current densities and efficiencies are calculated over each of the cell's internal area delimited by the scribing, which includes the Na/Al grid.

If not stated otherwise in the manuscript, PDTs were applied by evaporation of alkali fluorides in presence of Se vapor. The typical PDT sequence consisted of an initial NaF PDT followed by either KF as earlier described[1] or, similarly, RbF. The RbF deposition rate was approximately 1-2 nm/min. Standard PDT durations were 20 minutes for NaF and 20 minutes for RbF od KF. During the PDT, the KF and RbF sources cool at a rate of approximately 0.7°C/min. The evaporation rate decreased to approximately half by a temperature reduction of 20°C. Therefore, a prolongation of the KF or RbF

PDT from 20 to 30 minutes resulted in an approximate additional 30% amount of evaporated KF or RbF. A prolongation of the KF or RbF PDT from 20 to 60 minutes resulted in an approximate additional amount of evaporated KF or RbF of 120%.

Secondary Ion Mass Spectrometry (SIMS) depth-dependent compositional analysis was measured with a ToF-SIMS^5 unit by ION-TOF, using Bi as a primary positive ion source (25 keV, 1 pA) and a time-of-flight mass spectrometer. Depth profiling was performed by O_2+ sputtering (2 keV, 400 nA). Measurement was performed on 100×100 μm^2 area and sputtering area for depth profiling was 300×300 μm^2.

Scanning Electron Microscopy (SEM) micrographs were acquired in a Hitachi S-4800 SEM (acceleration voltage 5 keV, working distance 4 mm) on CIGS surfaces with an approximately 1 nm-tick Pt coating.

X-ray Photoelectron Spectroscopy (XPS) core levels were measured with a monochromated Al Kα source (1486.6eV) in a fixed analyzer transmission mode in a Quantum 2000 instrument from Physical Electronics. Core level spectra were measured with pass energy of 93.9 eV with a step size of 0.5 eV/step and charge compensation. A mild pre-sputtering with Ar+ ions at 0.5 keV for approximately 20s to 30s was applied before acquiring the spectra to remove surface contaminants. Preferential sputter etching is possible and could alter the surface stoichiometry. However, no attempt to quantify the surface composition is made, and the qualitative interpretation is verified by comparison with measurements performed on non-sputter-cleaned surfaces. The measurements on non-sputter cleaned surface exhibit the same trends and are not shown due to their poor signal-to-noise ratios.

In the ICP-MS measurements of Fig. 2 a) and b), atomic concentrations were measured on CIGS detached from the substrate at the Mo/CIGS interface. For the experiments shown in Fig.2 c) and d), atomic concentrations were measured in full PI/Mo/CIGS stacks. Samples of approximately 1 cm^2 were either rinsed in an aqueous solution of 10 mL of diluted NH_3 (2M) (Sigma-Aldrich, ≥99.99% trace metals basis) or also etched with a 3 M HCl solution (Alfa Aesar, ≥99.99% trace metals basis), in both cases for dipping times of 1 min. The rinsing procedure was chosen to mimic our standard solar cell processing sequence, i.e. immersion of the sample in the diluted ammonia bath immediately preceding the CdS deposition by CBD. Measurements were performed on as-deposited absorbers and after the rinsing and etching processes. The chemical composition of the PI/Mo/CIGS samples was measured by Triple Quadrupole Inductively Coupled Plasma Mass Spectrometry (QQQ-ICP-MS) and Inductively Coupled Plasma Optical Emission Spectroscopy (ICP-OES). The matrix elements (Cu, In Ga, and Se) were subjected to wet chemical extraction by means of HNO_3 67% Merck ultrapur and H_2O_2 30% Merck suprapur at room temperature. The solutions were diluted to 25 mL in ultrapure water pre eluted plastic vials, with ultrapure water and directly quantified by ICP-OES under the use of certified element standard materials, using a VARIA VISTA Pro Radial measurement unit. Alkali elements were measured by ICP-MS after further dilution of 1:10, in the O_2 reaction mode, with an Agilent 8800 triple quadrupole measurement unit under the use of certified element standard materials. For the first sample series with RbF PDT (fig. 2 c)), the Se concentration was not measured. In this case, atomic concentrations of alkali elements were calculated assuming a stoichiometric amount of Se in the CIGS. The assumption is validated by previous measurements, indicating that Se is always present in stoichiometric amounts with respect to Cu, In and Ga. No significant amounts of matrix elements are present in the molybdenum back contact layer as observed by SIMS. The

measurement and sample preparation accuracies were tested by analysis of ultrapure water-eluted empty deposition vials and standard reference material with no intentional deposition of alkali containing compounds.

The external quantum efficiency (EQE) response was measured with an in-house built system equipped with a halogen lamp light source and a monochromator (triple grating), chopped with a frequency of 260 Hz. The measurements were carried out under bias illumination with an intensity of approximately 100W/m^2. The solar cell temperature was kept constant at 25°C using PID-controlled Peltier heat pumps. The spectra calibration was performed by comparing the spectral response of a Si cell with a certified spectral response.

Results and Discussion

1. Solar cell performance

Table 1 compares the J-V parameters of solar cells based on CIGS absorbers layers treated with different PDTs. Individual cells were selected from samples with similar Cu concentration and [Ga]/([Ga]+[In]) (GGI) grading in the absorber. Absorbers with average GGI values between 0.34 and 0.36 are used, as determined by the intensity XRF. Typical [Cu]/([Ga]+[In]) ratios range between 0.88 and 0.92. The minimum bandgap was determined by linear extrapolation of the Tauc plot ((photon energy x EQE)^2 vs photon energy) for values between 25% and 75% of the EQE maximum. An uncertainty for such derived energy band gap values of 10 meV is estimated. It is important to ensure similar response of the EQE in the near-infrared (NIR) region, in order to minimize the impact of possible systematic errors in the determination of the minimum bandgap. The V_{oc} deficit of the different cells, calculated as the minimum bandgap minus the V_{oc}, is also given in Table 1.

Table 1. J-V parameters of solar cells grown on CIGS absorbers with different PDTs, comparing NaF only, NaF+KF and NaF+RbF. Values are given for the best cell and for the average of the four cells with the highest efficiency in each six-cell sample. The standard deviation is reported on average values only if larger than the estimated uncertainty on a single-cell measurement.

Post-deposition treatment	Eg (±0.01)[eV]	V_{oc} deficit (±0.01) [eV]	V_{oc} (±0.002) [V]	FF(±0.2) %	J_{sc}(±0.3) [mA/cm^3]	η (±0.3)%
NaF only	**1.16**	**0.46**	**0.696**	**76.3**	**33.6**	**17.9**
Average sample			*0.695*	*76.5(±0.4)*	*33.2*	*17.6*
NaF+KF*	**1.14**	**0.42**	**0.718**	**76.8**	**35.9**	**19.9**
Average sample			*0.719*	*76.8(±0.3)*	*35.6*	*19.6*
NaF+RbF	**1.15**	**0.43**	**0.716**	**77.3**	**35.7**	**19.7**
Average sample			*0.717*	*77.6(±0.3)*	*35.2(±0.5)*	*19.6*

***NaF+KF best cell J-V parameters already shown in a different context in an earlier publication [17].**

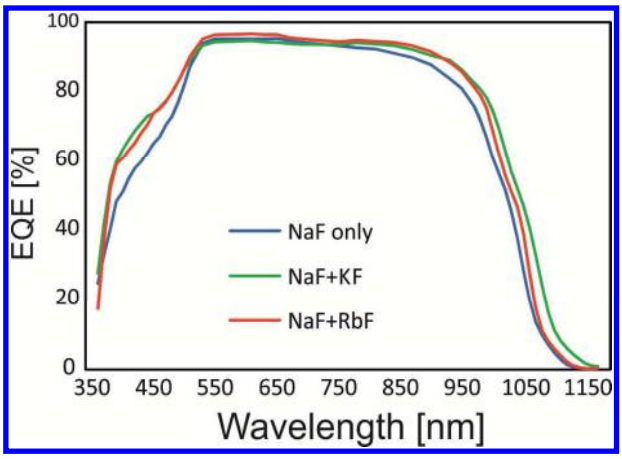

Figure 1 . EQEs of solar cells presented in Table 1.

All cells with NaF+KF and NaF+RbF PDTs show an improved efficiency in comparison to the cell treated with NaF PDT only, due to increased Jsc, FF and Voc. A V_{oc} deficit of (0.46±0.01) V was measured on the NaF-only PDT reference cell, whereas lower V_{oc} deficits of (0.42±0.01) V and (0.43±0.01) V were measured on samples treated with respectively NaF+KF and NaF+RbF PDTs. The V_{oc} deficit of the NaF+KF cell is partly compensated by a FF of 76.8. This results in efficiencies of (19.9±0.3) % for the KF treated cell and of (19.7±0.3) % for the RbF treated one. The NaF-only PDT reference has an efficiency of (18.9±0.3) %. For this cell a lower J_{sc} originates from a reduced response in the UV region due to the thicker buffer layer necessary when the NaF-only PDT is applied. Also, the J_{sc} is reduced by a decreased EQE response (shown in Fig.1) in the near-infrared, due to a possible incomplete photocarrier collection.

Table 2. J-V parameters of solar cells grown on CIGS absorbers with different NaF+RbF PDTs, comparing different durations and evaporation rates of RbF. Values are given for the best cell and for the average of the four cells with the highest efficiency in each six-cell sample. The standard deviation is reported on average values only if larger than the estimated uncertainty on a single-cell measurement.

Post-deposition treatment	Estimated additional RbF	CdS thickness	Eg (±0.01) [eV]	V_{oc}deficit (±0.01) [eV]	V_{oc}(±0.002) [V]	FF (±0.2) %	J_{sc} (±0.3) [mA/cm^3]	η (±0.3)%
NaF+RbF (standard 20+20 min)	standard	Standard thin	**1.16**	**0.44**	**0.723**	**77.8**	**32.6**	**18.4**
Average sample					*0.722*	*77.6(±0.4)*	*32.4*	*18.2*
NaF+RbF(20 min +30 min)	+30%		**1.16**	**0.45**	**0.711**	**75.9**	**33.2**	**17.9**
Average sample					*0.71*	*75.7*	*33.1*	*17.8*
NaF+RbF(20+ 20 min, RbF source +20°C)	+100%		**1.15**	**0.47**	**0.676**	**72.0**	**34.5**	**16.8**
Average sample					*0.672(±0.03)*	*70.6(±1.0)*	*34.7*	*16.5*

Table 2 shows the photovoltaic properties of solar cells based on absorbers treated by NaF+RbF PDT with variations of the RbF evaporation time and rate. The results are compared to a reference (standard 20min+20min, i.e. 20min NaF + 20min RbF) corresponding to the baseline process for RbF

PDT. In order to reduce as much as possible the effects of unwanted fluctuations in the multilayer quality, all samples in Table 2 belong to the same sample series (consecutive CIGS growth runs, same CBD bath and ARC deposition, equivalent parameters for the ZnO-based window layers). Larger amounts of RbF were evaporated by either a longer evaporation time and by a larger RbF evaporation rate. In the first case, the RbF PDT duration was prolonged by 10 minutes. Considering the cool-down of the RbF source during the PDT, this results in an additional amount of evaporated RbF of approximately 30% as compared to the standard. The larger evaporation rate was obtained by increasing the source temperature by 20°C. This corresponds to a doubling of the RbF evaporation rate.

The V_{oc} deficit increases with larger amounts of RbF, from (0.44 ±0.01) V of the reference to (0.45 ±0.01) V and (0.47±0.01) V for the longer PDT time and a larger RbF evaporation rate, respectively. The FF is reduced from (77.8±0.2)% to (75.9±0.2)% and (72.0±0.2)%. The efficiency is reduced from (18.4±0.3)% of the reference to (17.9±0.3)% and (16.8±0.3)%.

Previously reported results[1] and the results above show that, by adding suitable amounts of KF or RbF during PDTs, the V_{oc} deficits are reduced by approximately 30 to 40 mV, and the FFs are increased by 1-2% absolute compared to cells with a NaF PDT only. Furthermore, as reported earlier, the additional KF treatment allowed a reduction of the CdS layer thickness without losses in the FF and V_{oc}[1,10]. This led to an increased J_{sc} due to reduced parasitic absorption. Similarly reduced buffer layer thicknesses are also possible in the case of NaF+RbF PDTs. Further reductions of the buffer layer thickness result in degraded performance and non-reproducible behavior, both for KF and RbF PDTs (not shown here).

Similarly to the case of KF[7], degraded FF and V_{oc} are observed when too much RbF is added by either increasing the evaporation rate or the PDT duration. As previously observed[7], KF PDT results in the formation of a barrier for the injection current, which can in some cases lead to significant deterioration of the V_{oc} and FF. In the case of RbF, the formation of a similar barrier is also suspected, which counter-balances the beneficial effects of RbF PDT when too much RbF is added. A detailed study of such barrier behavior will be published elsewhere. Slightly increasing or decreasing the amount of RbF added by PDT does not significantly affect the solar cell performance. Similar J-V parameters could be obtained for RbF PDT durations between 15 min and 25 min, corresponding to approximate variations of respectively -17% and +19% in the total RbF added, with respect to the standard process (20 min). Further reductions of the amount of RbF lead to solar cell performances approaching those obtained by NaF PDT only (results not shown here).

According to the first-principle calculations, a segregation of a $KInSe_2$ layer is expected as a consequence of KF PDT[16]. Such compositional modification of the surface was experimentally observed for KF-treated CIGS layers[10]. As reported above, RbF PDT leads to improvements in the solar cell properties similar to those achieved with KF PDTs, and also allows similar reductions of the CdS buffer layer thickness. It is obvious, therefore, that comparable modifications of the chemical environment might be occurring at the surfaces of CIGS layers treated by KF PDT and by RbF PDT. Recently published DFT calculations suggest the formation of a $KInSe_2$ or a $RbInSe_2$ phase segregating at the surface under typical PDT conditions [16]. No segregation of secondary phases during NaF PDT is expected. In the following, compositional and morphological analysis of CIGS layers is presented, comparing NaF-only, NaF+KF and NaF+RbF PDTs, in order to provide experimental evidence for the theoretical predictions. CIGS layers are analyzed by ICP-MS and XPS after different surface chemical

treatments. The distribution of alkali elements in the absorbers is analyzed by SIMS and TEM/EDX. ICP-MS/OES and XPS results obtained on absorber treated with KF were previously shown[10] and are presented again here to allow for direct comparison with the corresponding measurements concerning PDTs with RbF.

2. Compositional and morphological modifications of CIGS thin films induced by post deposition treatments with alkali fluorides

The ICPMS measured concentrations of alkali elements in CIGS films with different PDTs and surface treatments and are shown in Fig. 2. The measurement error is estimated from the amount of external contamination measured in empty sample preparation vials if available. Else, the detection limit is given to underline the confidence in the data.

For comparison with earlier findings, previously published results are added in Fig.2 a) and b)[10]. These results concern the effects of NaF and KF PDTs and are compared with original results on RbF PDTs in Fig.2 c) and d).

In the ICP-MS measurements on KF-treated absorbers (Fig. 2 a) and b)), the CIGS layer was removed from the PI/Mo substrate before the measurements. In the measurements on Rb-treated absorbers (Fig. 2 c) and d)), the substrate was not removed from the CIGS: as alkali elements accumulate in the molybdenum layer, an overestimation of the alkali concentrations is possible. This unwanted additional amount of alkali elements cannot be affected by the surface treatments (rinsing and etching), since the Mo layer is buried between the CIGS and the PI substrate. To avoid erroneous interpretations, the discussion of ICP-MS results only compares the relative differences in the Na, K and Rb concentration between pieces of the same absorber with different surface treatments (i.e. before and after the rinsing and etching steps).

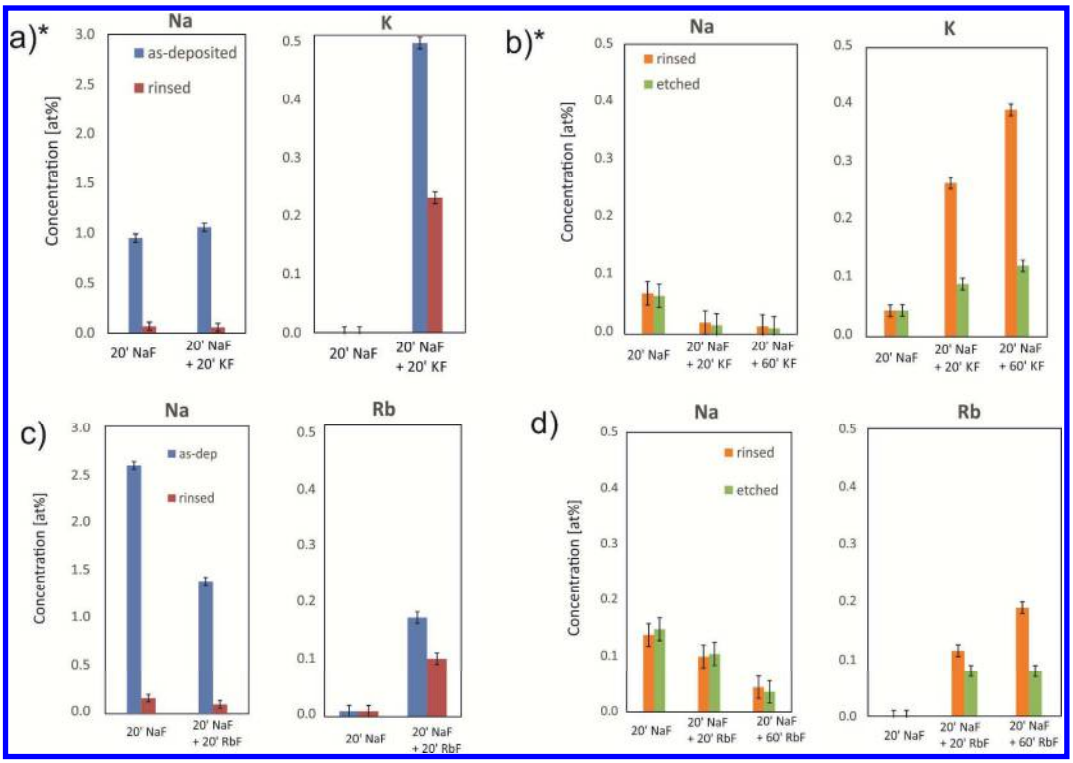

*previously partially shown by Reinhard *et al.*[10]

Figure 2. Concentrations of Na, K and Rb in CIGS films treated with different PDTs, measured by ICP-MS on as-deposited absorbers, after rinsing with diluted ammonia (2 M) and after etching with diluted HCl (3 M). In Fig. a) and b), the CIGS was removed from the PI and molybdenum substrate before the measurement, whereas the concentrations reported in Fig. c) and d) include possible contamination of the substrate with alkali elements.

Fig.2 a) shows a comparison of alkali concentration in CIGS layers treated by NaF-only and NaF+KF PDTs, measured before and after rinsing with diluted ammonia. In layers without rinsing, the Na concentration is approximately 1 at.%. K concentrations are below the detection limit in the NaF PDT sample and 0.5 at.% in the NaF+KF PDT sample. In the rinsed layers, the Na concentrations drop but a significantly larger potassium concentration is measured in KF treated layers.

In a separate experiment (Fig.2 b)), three different PDTs were compared: NaF only (20 min), NaF+KF (20 min and 20 min), and a modified NaF+KF (KF PDT increased to 60 min). Na and K concentrations were measured in layers after rinsing and after etching with diluted HCl. In the rinsed layers, Na concentrations are (0.07±0.04) at.% for the sample with NaF-PDT only and below the detection limit for the samples with additional KF. Potassium concentrations are (0.04±0.01) at.% for the sample with no intentional KF, and respectively (0.26±0.01) at.% and (0.39±0.01) at.% for the samples with shorter and longer KF PDT. In the layers etched with HCl, Na concentrations are unchanged in all samples, but potassium concentrations are reduced significantly.

Fig.2 c) shows elemental concentrations measured on samples treated by NaF PDT only and by NaF+RbF PDT. The alkali concentrations were measured on as-deposited absorbers and after rinsing with diluted ammonia. In the as-deposited samples, Na concentrations above 2.5 at.% and 1.5 at.% are measured respectively for the samples with and without intentional RbF. The Na concentration is reduced by the rinsing to 0.162 (±0.02) at.% in the sample with NaF PDT and to (0.10 ± 0.01) at.% in

the sample treated with NaF+RbF PDT. Rb concentration is always below the detection limit in the sample with no intentional Rb addition. In the sample with additional RbF PDT, the Rb concentration is reduced from (0.17 ± 0.01) at.% before the rinsing to (0.10±0.01) at.% after.

In Fig.2 d), ICP-MS measurements on samples with NaF PDT followed by a standard (20 min) and longer (60 min) RbF PDT are presented. Similarly as in the experiments illustrated in Fig.2 b), alkali elements are measured in layers after rinsing with diluted ammonia and after etching with diluted HCl. The Na concentration is equal in rinsed and etched layers. Na concentrations of respectively (0.10±0.01) at.% and (0.04±0.01) at.% were measured in the samples with the shorter and longer additional RbF PDT. In rinsed samples, the Rb concentration is (0.11 ± 0.01) at.% for the shorter RbF evaporation time and (0.19±0.01) at.% for the longer one. The etching step reduces the Rb concentration to equal values of (0.8±0.01) at.%.in both samples.

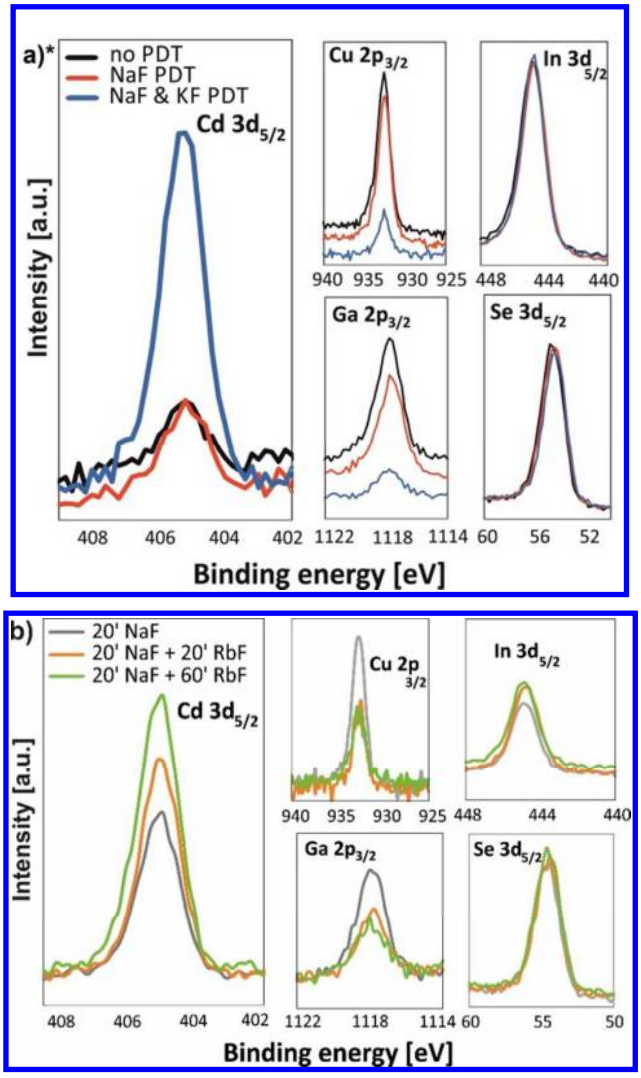

*previously shown by Reinhard *et al.*[10]

Figure 3. XPS core-level intensities of matrix elements on CIGS surface dipped in a diluted ammonia solution with Cd acetate. a) already shown[10], measurements performed on CIGS samples with no, NaF and NaF+KF PDTs. b) Same peak intensities measured on samples CIGS samples with NaF, NaF+RbF, and NaF+ longer RbF PDTs.

Further characterization of the surface composition was performed by XPS on samples treated by different PDTs. The samples were dipped for approximately 20 min in a diluted ammonia solution with cadmium acetate. Cd acetate is typically used as the source of Cd^{2+} ions in the deposition of the CdS buffer layer. Results in Fig. 3 a) were previously shown and discussed[10], and are re-discussed here for comparison with the experiments concerning RbF PDT.

In Fig. 3 a), XPS core level intensities are compared between CIGS absorbers treated with PDT, NaF PDT and NaF+KF PDTs. The In $3d_{5/2}$ and Se $3d_{5/2}$ intensities are similar for all samples. The Cu $2p_{3/2}$ and the Ga $2p_{3/2}$ core level intensities are similar in the cases of no- and NaF- PDT, but greatly reduced in the sample with additional KF PDT. The Cd $3d_{5/2}$ peak intensity is also similar for the cases of no- and NaF- PDT, and strongly increased on the sample with additional KF. In Fig.3 b) the XPS core level intensities are compared between a sample treated by NaF PDT, and samples with NaF PDT followed by a standard (20 min) and longer (60 min) RbF PDT. The Se $3d_{5/2}$ peak is similar for all samples. The In $3d_{5/2}$ intensity is slightly more intense on the two samples with RbF PDT, as compared to the NaF-only reference. The Cu $2p_{3/2}$ and Ga $2p_{3/2}$ core level intensities are reduced on the samples with RbF. In, Cu and Ga peaks do not show significant differences when comparing the samples with the shorter and longer RbF PDT. The Cd $3d_{5/2}$ core level intensity is lowest in the sample with no intentional Rb addition, and increases with increasing RbF evaporation time.

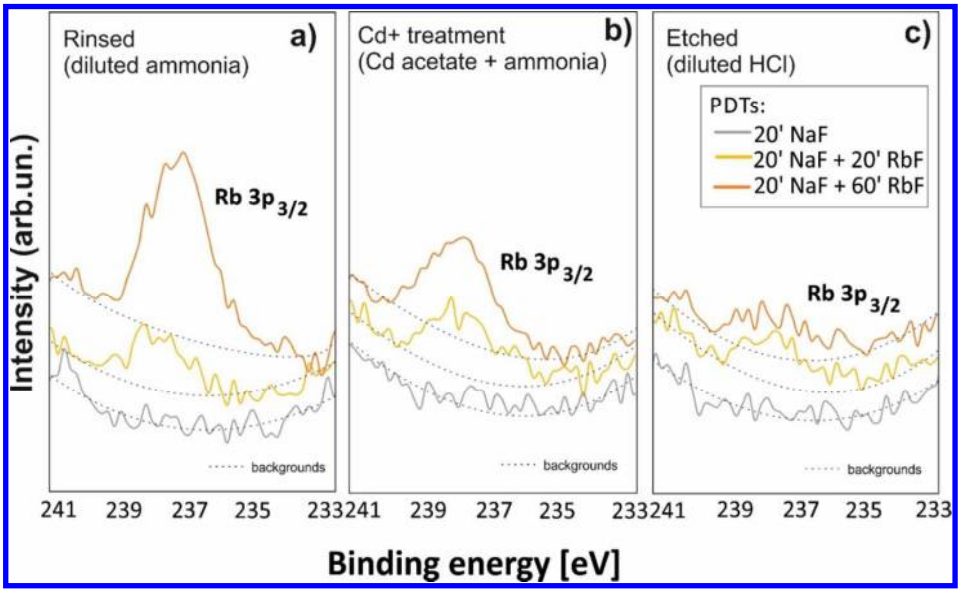

Figure 4. XPS peak intensity of the Rb $3p_{3/2}$ core-level in a) absorbers washed in diluted ammonia b) absorbers treated by a Cd+ ion bath and c) absorbers treated with a diluted HCl solution.

The Rb $3p_{3/2}$ core level intensity was measured by XPS on the sample series presented in Fig. 2 d) and in Fig. 3 b). Fig. 4 shows a comparison of the Rb intensity after the samples were rinsed with diluted ammonia, after a bath in diluted Cd acetate, and after ammonia rinsing plus etching by diluted HCl. A poor signal to noise ratio is obtained due to relatively low Rb concentration. As expected, the Rb $3p_{3/2}$ peak cannot be distinguished from the background noise for the sample with no intentional Rb addition. The appearance of a Rb $3p_{3/2}$ peak can be observed in the samples with intentional RbF PDT and rinsed in diluted ammonia. The peak is more intense for the sample with the longest RbF PDT duration. Similar trends in the Rb $3p_{3/2}$ peak are observed in the samples dipped in the Cd^{2+} ion bath, although with a reduced peak intensity, especially in the case of the sample with the longest RbF PDT. Significant amounts of Rb remain therefore on the surface even after the Cd-ion treatment. On

the samples treated by HCl, only a small Rb $3p_{3/2}$ signal can be distinguished from the background for the two samples with RbF.

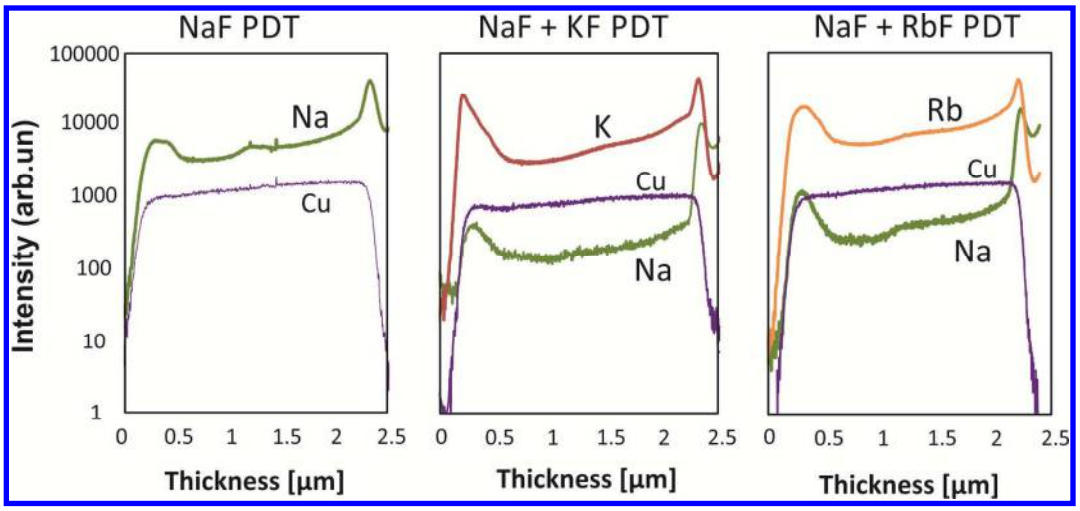

Figure 5. SIMS depth profiles signals from Na, K, Rb and Cu in samples treated by NaF PDT (top), NaF and KF PDT (bottom-left) and NaF and RbF PDT (bottom-right).

The distribution of alkali elements throughout the thickness of CIGS thin films was investigated by SIMS depth profiling. Fig.5 shows SIMS profiles of samples with NaF, NaF+KF, and NaF+RbF PDTs. The Cu profile is shown as a reference matrix element to guide the eye for the relative changes in the intensities of alkali element. The samples have similar [Cu]/([Ga]+[In]) ratios of approximately 0.9 as measured by XRF. No significant change in the Cu distribution is expected throughout the sample thickness. A small increase of the Cu signal from the front to the back of the absorber is observed, which could be the consequence of forward implantation of Cu atoms during the sputtering with O_2+ ions A small variation in the Cu concentration throughout the film thickness cannot be ruled out, which will be subject of further investigation in the future. A similar effect on the alkali elements cannot be excluded. All alkali elements tend to accumulate at the front and the back interfaces of the absorbers, with somewhat lower concentrations in the center. The majority of alkali elements are expected at surfaces and grain boundaries but a small alkali accumulation can also be observed in the central region of each layer. The accumulation at the front appears to be relatively smaller for Na in the NaF PDT layer and larger for K and Rb in the NaF+KF and in the NaF+RbF layers, respectively. Especially, in the sample treated with Na+KF PDT, a very strong peak of the K signal can be observed. Na and Rb show instead smoother front distributions. The Na signal is reduced by more than one order of magnitude in the samples with additional KF or RbF PDTs, despite an initial NaF PDT in all of the three samples with equal duration.

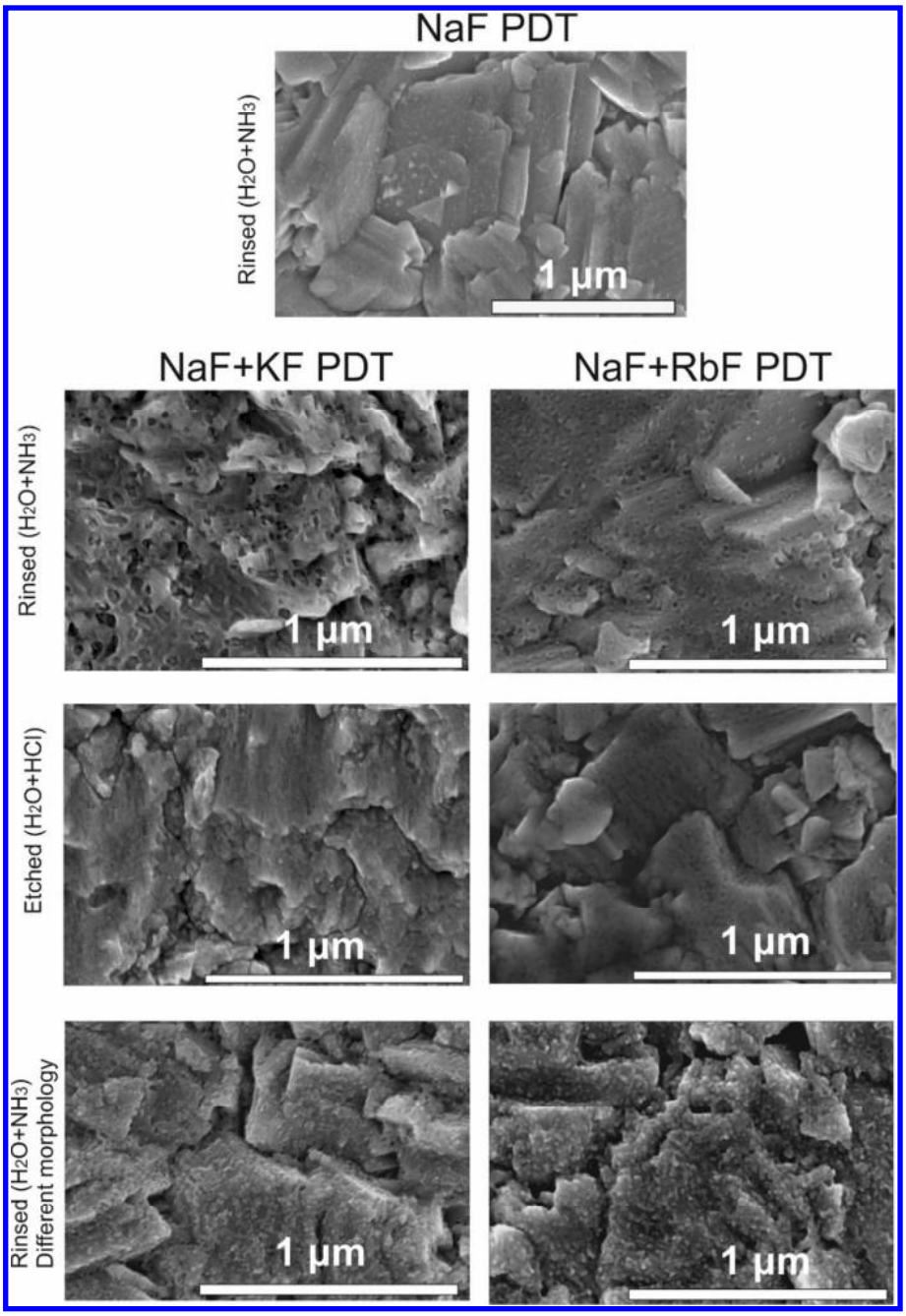

Figure 6. SEM top-view images of CIGS thin films treated by NaF PDT, NaF+KF PDT, and NaF+ RbF PDT. Samples were rinsed in diluted ammonia (H_2O+NH_3) or etched with a diluted H_2O+HCl solution, as specified in the figure.

SEM micrographs of the CIGS surface are shown in Fig.6 after different PDT treatments. The surface of NaF PDT CIGS layers after rinsing appears smooth and similar to the surface of absorbers without any PDT (not shown), as previously reported[11]. A significantly altered morphology can be observed on the surfaces of the layers treated by NaF+KF and NaF+RbF. In both cases, patterned surfaces are observed. The patterning features on the RbF-treated surface appear smaller (approx. 10 nm) than for the KF treatment (30-50 nm). The size and distance of the patterning can be heavily influenced by the CIGS deposition and PDT parameters, as described below. After etching the CIGS surface for 1 min with a 3 M HCl solution, the patterning is completely removed in the case of KF and partially

removed in the case of RbF. In the latter case, the features appear blurred and less defined than after rinsing. An apparent blurring of a specific surface morphology could be affected by SEM-related artifacts. However, the SEM micrographs showing comparison of layers with or without HCl etching were acquired in the same measurement session without breaking the vacuum and with no change in the stigmation and contrast parameters. Comparable quality of the focusing was verified by similar definition of the grain edges. Etching of RbF-treated surfaces with a more concentrated HCl solution (6 M) resulted in further fading of the patterned morphology (not shown).

On KF- and RbF-treated surfaces, patterned layers with significantly different morphologies were also observed in rinsed layers. Two examples (for KF and RbF PDTs) are given at the bottom of Fig. 6. In these cases, the surface patterning appears like a precipitate of nanosized grains, with diameters of 10 to 20 nm.

3. Discussion

The reduction of the alkali concentrations in rinsed layers, measured by ICP-MS, is consistent with the dissolution in water or dilute ammonia of alkali fluoride crystals accumulated on the CIGS surface, which was previously shown in the case of NaF and NaF+KF PDTs[11]. Relatively to the total amounts added by PDTs, nearly all of the Na is reduced (dissolved) by rinsing to concentrations in the order of the reported solubility limit of Na in polycrystalline CIGS thin films (0.1 to 0.2 at.%). Lower amounts of K and Rb are removed by the rinsing relatively to the concentrations measured on non-rinsed absorbers (total amounts added by the PDT). Compared to Na, larger parts of the K and Rb added by PDTs remain therefore incorporated in compounds that cannot be washed away by rinsing with diluted ammonia. SIMS measurements indicate that a large part of potassium and Rb accumulate mostly close to the CIGS front surface. The Na concentrations measured are lower in samples with additional KF or RbF PDTs, which is in line with the previously reported ion exchange mechanism[1]. Both K and Rb tend therefore to partially substitute Na during KF or RbF PDTs.

Rb concentrations in PI/Mo/CIGS stacks increase with increasing RbF evaporation time (Fig. 2 d)) both in as-deposited and in rinsed absorbers. The amount of Rb removed by etching is larger in the sample with a longer RbF evaporation time. This confirms the presence of a Rb-rich surface layer that can be completely or partially removed by HCl etching. The amount of Rb accumulated in this surface layer increases with increasing duration of the RbF PDT.

Due to a possible overestimation of the Rb concentration (potential incorporation of Rb in the PI/Mo substrate) in ICP-MS measurements, it is not possible to quantify the exact concentration of Rb incorporated at the surface layer and in the bulk of the CIGS. An upper limit can however be given. After rinsing in diluted ammonia, Rb is present in maximal concentrations of approximately 0.1 at.% for the standard RbF PDT and 0.2 at.% for the longer one. After etching the Rb-rich surfaces with diluted HCl, the maximal Rb concentration in the CIGS layer is found independent of the RbF PDT duration, indicating that the Rb accumulates in the CIGS layer up to a given solubility limit which does not depend on the PDT duration. These results also suggest that additional amounts of Rb accumulate at the surface in compounds that can be etched away by diluted HCl. An analogous behavior is observed for potassium in KF-treated absorbers (Fig. 2 a) and b))[10].

The XPS Rb $3p_{3/2}$ peak intensities confirm that the amount of Rb at rinsed CIGS surfaces increases with increasing RbF evaporation time. The peak is strongly reduced after HCl etching, independently of the PDT duration. This confirms that a Rb-rich surface layer can be completely or partially etched out by diluted HCl. No fluorine core-level signal could be distinguished from the background in any of the samples measured by XPS , indicating that the rinsing procedure efficiently removes the fluorine-rich compounds present on the surface after PDT. XPS results also indicate that RbF PDT induces Cu and Ga depletion at the CIGS surface. After the Cd^{2+} ion treatment, the Cd concentration at the CIGS surface is larger for the layers treated with RbF, as indicated by the core level intensities of Cd $3d_{5/2}$. A similar result was previously observed for KF PDT. The XPS measurements of Fig.4 show that, after the Cd^{2+} ion bath, a significant amount of Rb is still present at the surface. It was recently suggested by Lepetit[9] that the alkali elements could be substituted by Cd during CdS CBD. A complete substitution of Rb by Cd at the surface is not observed after the treatment with Cd^{2+} ions, however, a partial substitution cannot be excluded.

RbF PDT leads therefore to the formation of a Rb-rich, Cu-poor and possibly indium-rich and Ga-poor surface. The Cd surface enrichment is likely to occur also during the first minutes of the deposition of CdS by CBD, when no heterogeneous nucleation of CdS takes place yet but Cd^{2+} ions are available in the CBD solution. These trends in the XPS core-level intensities of Cu, Ga, In and Cd are also observed for KF PDT, as already discussed[1,10], and presented again for comparison in Fig.3.

As observed in the SEM micrographs, both RbF and KF PDTs induce a change in the morphology of the surface, with the appearance of a nanopatterning (Fig. 6). As previously reported for KF PDT layers,[11]the nanopatterned surface was associated with the presence of a layer of a different phase, namely "KIS" (potassium- and indium- rich, Cu poor, possibly $KInSe_2$). The K-rich phase could be completely etched away by HCl (3 M for 1 min). Different patterned morphologies can be observed both in the case of RbF and KF PDTs. The patterning can appear as a homogeneous layer with nanosized holes or also as a precipitate of nanocrystals on the surface. The morphology strongly depends on the deposition and PDT conditions, such as the Se pressure and the Cu concentration in the CIGS. With the concentrations and etching times used in these experiments (1 min, 3 M) the patterned morphology of RbF-treated surfaces does not vanish completely after the HCl treatment. A blurring and apparent partial vanishing of the patterning is observed. The Rb-rich surface layer seems to be more resistive to HCl etching than the corresponding K-rich surface layer induced by KF PDT, which completely disappears after etching with diluted HCl (3 M) for 1 min.

As observed in SIMS measurements (Fig.5), alkali elements accumulate close to the CIGS/CdS interface. This is more pronounced for K and Rb than for Na. Particularly, in absorbers treated by KF PDT, the measurement signal for K shows a spike-like behavior[10]. No similar shape of the Rb signal is observed on RbF-treated samples, but rather a smoother distribution with a maximum in the surface region. The larger concentration of all alkali elements close to the front surface is expected due to the presence of smaller grains (larger concentration of grain boundaries) in the front region of the CIGS absorbers, as observed by SEM cross section (not shown). At the very front of the CIGS layer, the sharpness of the front peak of the potassium signal was previously described[10]. The Rb signal plot in RbF-treated absorbers does not have such a sharp shape. The SIMS signals at an interface can be influenced by the different sputtering yields for Rb and K and by different implantation yields for recoil and cascade mixing, which may lead to apparent interface broadening[18] and may differ depending on the atomic weight of the elements at the surface. Due to such possible artifact, it is

difficult to give an unequivocal interpretation to these results in terms of segregation of an alkali-rich phase at the surface.

After RbF PDT and KF PDTs, Rb and K are present in significant amounts also within the polycrystalline CIGS layer (at the grains or at grain boundaries). The Na signal is significantly lower than in the case of NaF PDT only. Therefore, both K and Rb substitute Na atoms in the bulk of the CIGS during PDTs. Such ion-substitution mechanism was previously described for KF PDT[1].

The segregation of Rb- or K- rich, Cu-poor phase at the surface following RbF or KF PDTs can be corroborated by the results of first-principle calculation. In particular, Malitckaya *et al.*[16] investigated secondary phase formation in CIS ($CuInSe_2$) during PDTs with alkali fluorides in Se atmosphere. The formation energies of $AlkInSe_2$ phases were calculated (where Alk stands for alkali elements, under consideration were Li, Na, K, Rb and Cs). Malitckaya *et al*. performed DFT calculations using the VASP program package on 128-atoms supercells, assuming that initially alkali fluorides react with Se to form alkali selenides, and then alkali selenides react with the CIGS matrix. They found, that the reaction of alkali selenides with $CuInSe_2$ to form $AlkInSe_2$ compounds is energetically favorable only in the case of K, Rb and Cs, and not in the cases of Li and Na, which tend to remain a volatile Alk_2Se phase. The formation of mixed $CuInSe_2$-$AlkInSe_2$ phases was also investigated[16]. Mixed phases can occur both by reaction between $CuInSe_2$ and $AlkInSe_2$ phases and by substitution of pre-existing Cu vacancies by alkali elements at the CIGS Cu-poor surface regions. Whereas Rb and Cs do not mix, potassium may, in concentrations up to 0.6 at% at PDT temperatures, be incorporated by substitution of Cu vacancy. However, positive formation energies for the mixed phase were calculated only for Li and Na. Instead, K-, Rb- and Cs-based $AlkInSe_2$ tend to segregate. Mixed $Cu_{(1-x)}Alk_xInSe_2$ phases are not stable and phase separation is expected to occur at typical PTD temperatures of 350°C, with exceptions for Li and Na at low concentrations ($x < 10^{-3}$, i.e. 0.1 at %).

$AlkInSe_2$ phases are therefore expected to be found at the surface after PDT in the cases of K, Rb and Cs, either by reaction with $CuInSe_2$ at the CIGS surface with segregation of Cu_2Se, or by segregation of mixed $CuInSe_2$ and $AlkInSe_2$ phases. Lithium behaves similarly as sodium. The $KInSe_2$ and $RbInSe_2$ phases could correspond to the alkali-rich, Cu-poor layer observed on the surface of KF- and RbF-treated absorbers.

Conclusions

CIGS layers were deposited by low-temperature multi-stage co-evaporation and subsequently post deposition treatments with alkali fluorides were applied. J-V parameters indicate that the RbF PDTs and KF PDT similarly improve the performance of solar cells based on low-temperature co-evaporated CIGS thin films. The benefits of RbF and KF PDT consist in increased open circuit voltages and fill factors. Excessive amounts of RbF or KF result instead in degraded photovoltaic properties. The thickness of the CdS layer can be reduced without loss of photovoltaic properties if KF or RbF PDTs are applied. The allowed thickness reduction is similar for both KF and RbF, with similar gains in short circuit current densities.

The mechanisms which lead to improved solar cell performance are very similar for RbF and KF. In both cases, the CIGS surface is depleted of Cu and enriched with Rb or K, as measured by XPS and ICP-MS and earlier already reported for KF PDTs[10]. These results experimentally corroborate the predictions of DFT calculations[16] that, during PDTs, secondary phases consisting of $RbInSe_2$ and $KInSe_2$ segregate at the CIGS surface. The segregation of such secondary phases at the CIGS surface results in a patterned surface morphology. Furthermore, both Rb and K substitute Na in the CIGS bulk.

Our analysis suggests that KF PDT and RbF PDT are equally effective in improving the performance of CIGS solar cells, due to similar mechanisms of chemical modifications of the CIGS surface and bulk. This conclusion is consistent with the theoretical predictions by Malitckaya *et al*[16].

Acknowledgements

This work was done in the framework of the European Unions's Horizon 2020 research and innovation program under grand agreement No 641004 (Sharc25) and funded by the Swiss State Secretariat for Education, Research and Innovation (SERI) under contract number REF-1131-52107.

Work is supported by the National Research Program 'Energy Turnaround' (NRP 70) of the Swiss National Science Foundation (SNSF) in the project "PV2050: Building blocks for next generation multi-Junction solar cells" under grant No 407040-153916; by the Swiss Federal Office of Energy (SFOE) under contact No SI/501145-01.

Dr. Shiro Nishiwaki (Empa), Benjamin Bissig (Empa) and Dr. Patrick Reinhard (Flisom AG) are gratefully acknowledged for their contribution in the interpretation of the results.

The Laboratory for Nanoscale Material Science at Empa is gratefully acknowledged for granting access to SIMS measurements facilities.

Notes

The authors declare no competing financial interest.

References

(1) Chirilă, A.; Reinhard, P.; Pianezzi, F.; Bloesch, P.; Uhl, A. R.; Fella, C.; Kranz, L.; Keller, D.; Gretener, C.; Hagendorfer, H.; *et al.* Potassium-Induced Surface Modification of Cu(In,Ga)Se2 Thin Films for High-Efficiency Solar Cells. *Nat. Mater.* **2013**, *12*, 1107–1111.

(2) Jackson, P.; Wuerz, R.; Hariskos, D.; Lotter, E.; Witte, W.; Powalla, M. Effects of Heavy Alkali Elements in Cu(In,Ga)Se2 Solar Cells with Efficiencies up to 22.6%. *Phys. Status Solidi - Rapid Res. Lett.* **2016**, *10*, 583–586.

(3) Rudmann, D.; Bŕmaud, D.; Zogg, H.; Tiwari, a. N. Na Incorporation into Cu (In,Ga) Se2 for High-Efficiency Flexible Solar Cells on Polymer Foils. *J. Appl. Phys.* **2005**, *97*, 10–15.

(4) Laemmle, A.; Wuerz, R.; Schwarz, T.; Cojocaru-Mirédin, O.; Choi, P.-P.; Powalla, M. Investigation of the Diffusion Behavior of Sodium in Cu(In,Ga)Se2 Layers. *J. Appl. Phys.* **2014**, *115*, 154501.

(5) Friedlmeier, T. M.; Jackson, P.; Bauer, A.; Hariskos, D.; Kiowski, O.; Wuerz, R.; Powalla, M. Improved Photocurrent in Cu(In,Ga)Se<inf>2</inf> Solar Cells: From 20.8% to 21.7% Efficiency with CdS Buffer and 21.0% Cd-Free. *IEEE J. Photovoltaics* **2015**, *5*, 1487–1491.

(6) Mansfield, L. M.; Noufi, R.; Muzzillo, C. P.; Dehart, C.; Bowers, K.; To, B.; Pankow, J. W.; Reedy, R. C.; Ramanathan, K. Enhanced Performance in Cu(In,Ga)Se2 Solar Cells Fabricated by the Two-Step Selenization Process with a Potassium Fluoride Postdeposition Treatment. *IEEE J. Photovoltaics* **2014**, *4*, 1650–1654.

(7) Pianezzi, F.; Reinhard, P.; Chirilă, A.; Bissig, B.; Nishiwaki, S.; Buecheler, S.; Tiwari, A. N. Unveiling the Effects of Post-Deposition Treatment with Different Alkaline Elements on the Electronic Properties of CIGS Thin Film Solar Cells. *Phys. Chem. Chem. Phys.* **2014**, *16*, 8843–8851.

(8) Pistor, P.; Greiner, D.; Kaufmann, C. a; Brunken, S.; Gorgoi, M.; Steigert, a; Calvet, W.; Lauermann, I.; Klenk, R.; Unold, T.; *et al.* Experimental Indication for Band Gap Widening of Chalcopyrite Solar Cell Absorbers after Potassium Fluoride Treatment. *Appl. Phys. Lett.* **2014**, *105*, 63901–63905.

(9) Lepetit, T. Influence of KF Post Deposition Treatment on the Polycrystalline Cu(In,Ga)Se2/CdS Heterojunction Formation for Photovoltaic Application. **2015**.

(10) Reinhard, P.; Bissig, B.; Pianezzi, F.; Avancini, E.; Hagendorfer, H.; Keller, D.; Fuchs, P.; Döbeli, M.; Vigo, C.; Crivelli, P.; *et al.* Features of KF and NaF Postdeposition Treatments of Cu(In,Ga)Se $_2$ Absorbers for High Efficiency Thin Film Solar Cells. *Chem. Mater.* **2015**, *27*, 5755–5764.

(11) Reinhard, P.; Bissig, B.; Pianezzi, F.; Hagendorfer, H.; Sozzi, G.; Menozzi, R.; Gretener, C.; Nishiwaki, S.; Buecheler, S.; Tiwari, A. N. Alkali-Templated Surface Nanopatterning of Chalcogenide Thin Films: A Novel Approach Toward Solar Cells with Enhanced Efficiency. *Nano Lett.* **2015**, 150408100833003.

(12) Khatri, I.; Fukai, H.; Yamaguchi, H.; Sugiyama, M.; Nakada, T. Effect of Potassium Fluoride Post-Deposition Treatment on Cu(In,Ga)Se2 Thin Films and Solar Cells Fabricated onto Sodalime Glass Substrates. *Sol. Energy Mater. Sol. Cells* **2016**, *155*.

(13) Handick, E.; Reinhard, P.; Alsmeier, J. H.; Köhler, L.; Pianezzi, F.; Krause, S.; Gorgoi, M.; Ikenaga, E.; Koch, N.; Wilks, R. G.; *et al.* Potassium Postdeposition Treatment-Induced Band Gap Widening at Cu(In,Ga)Se2 Surfaces - Reason for Performance Leap? *ACS Appl. Mater. Interfaces* **2015**, *7*, 27414–27420.

(14) Lepetit, T.; Harel, S.; Arzel, L.; Ouvrard, G.; Barreau, N.; Jean, M.; Imn, R.; Umr, C.; Nantes, M. De; Bp, H.; *et al.* Co-Evaporated KInSe 2 : A Fast Alternative to KF Post Deposition Treatment in High Efficiency Cu (In , Ga) Se 2 Thin Film Solar Cells. *Ieee Pvsc* **2016**, *6*, 2–5.

(15) Jackson, P.; Hariskos, D.; Wuerz, R.; Wischmann, W.; Powalla, M. Compositional Investigation of Potassium Doped Cu(In,Ga)Se2 Solar Cells with Efficiencies up to 20.8%. *Phys. Status Solidi - Rapid Res. Lett.* **2014**, *8*, 219–222.

(16) Malitckaya, M.; Komsa, H.-P.; Havu, V.; Puska, M. J. Effect of Alkali Metal Atom Doping on CuInSe 2 -Based Solar Cell Absorber. *J. Phys. Chem. C* **2017**, acs.jpcc.7b03083.

(17) Avancini, E.; Carron, R.; Bissig, B.; Reinhard, P.; Menozzi, R.; Sozzi, G.; Di Napoli, S.; Feurer, T.; Nishiwaki, S.; Buecheler, S.; *et al.* Impact of Compositional Grading and Overall Cu Deficiency on the near-Infrared Response in Cu(In, Ga) Se2 Solar Cells. *Prog. Photovolt Res. Appl.* **2017**, *25*, 233–241.

(18) Sigmund, P.; Gras-Marti, A. Distortion of Depth Profiles during Sputtering: 1. General Description of Collisional Mising. *Nucl. instruments Methods* **1980**, *168*, 389–394.

Insert Table of Contents artwork here